AIAA JOURNAL
Vol. 50, No. 4, April 2012

Modeling and Testing of a Semiactive Hydraulic Damper in Periodic Working Regimes

Branislav Titurus,* Jonathan du Bois,† and Nick Lieven‡
University of Bristol, Bristol, England BS8 1TR, United Kingdom

DOI: 10.2514/1.J051152

This paper presents analytical and experimental studies of a modified semiactive hydraulic damper operating in periodic working regimes. This work was completed as a part of the Rotor Embedded Actuator Control Technology project sponsored by the Technology Strategy Board in the United Kingdom. The damper tested is based on modifications to an industrially employed helicopter damper. The work presented covers the relevant aspects of the model development, damper modification, test planning, and analysis, as well as a model-simulation correlation study. The model of the damper directly reflects the actual hydraulic modification, enabling a semiactive mode of operation. Pressure-flow representations used in the damper modeling are based on a novel testing methodology using triangular piston excitation waveforms. A specific test structure based on varying the relative phase difference between two harmonic input signals is used to assess the damper properties in periodic working regimes. The test configuration with a base harmonic piston excitation combined with a harmonic modulation at a frequency 3 times higher than the base frequency leads to significant changes in the second and fourth harmonic components of the resulting periodic damper forces. A successful model-simulation correlation study suggests that a simple one-state dynamic model of this damper features good predictive properties, equally applicable in the extended simulation contexts.

Nomenclature

A_j, B_j	=	Fourier coefficients
A_P	=	cross-sectional area of the symmetric piston
A_V	=	cross-sectional area of the valve opening
$B_{0,\text{eff}}$	=	constant effective bulk modulus of a hydraulic fluid
C_D	=	discharge coefficient
C_L, C_Q	=	linear and quadratic pressure-flow coefficients
f	=	frequency
F_D	=	damper force
p	=	absolute and homogeneous pressure in the fluid container
Q	=	volumetric flow rate
q^{-1}	=	inverse of the function q
sign(∘)	=	signum function
T	=	fundamental period
t	=	time
V	=	volume of the fluid chamber
$\mathcal{V}$	=	auxiliary volume function
xR	=	number of the cycles per one revolution
x_V	=	valve spool displacement
y_P	=	piston displacement
$W_{\{i,j\}}$	=	work done per one cycle with ith excitation frequency and jth phase shift
β	=	isothermal tangent compressibility of the hydraulic fluid
Δp	=	pressure difference due to pressure losses
ρ	=	density of hydraulic fluid
φ	=	phase difference between damper piston and valve spool harmonic motions
ω	=	angular frequency of harmonic damper piston excitation
$\lvert \circ \rvert$	=	absolute value

Received 6 January 2011; revision received 20 October 2011; accepted for publication 22 October 2011. Copyright © 2012 by University of Bristol. Published by the American Institute of Aeronautics and Astronautics, Inc., with permission. Copies of this paper may be made for personal or internal use, on condition that the copier pay the $10.00 per-copy fee to the Copyright Clearance Center, Inc., 222 Rosewood Drive, Danvers, MA 01923; include the code 0001-1452/12 and $10.00 in correspondence with the CCC.

*Lecturer, Department of Aerospace Engineering, Queens Building, University Walk.

†Researcher, Department of Aerospace Engineering, Queens Building, University Walk.

‡Professor, Department of Aerospace Engineering, Queens Building, University Walk.

I. Introduction

THIS paper provides analytical and experimental studies of a hydraulic damper in a periodic operational regime. The studies are presented as a combination of laboratory experiments and simulations, with correlation studies between the two. The subject of the current study is a modified industrial hydraulic damper. The motivation behind this work is the improvement of our understanding of the operation of semiactive hydraulic dampers in periodic working conditions. These conditions are relevant to structural components located in systems exposed to sustained periodic excitation. These conditions are often induced in rotating systems such as rotors. One approach to damper modeling is low-order physics-based modeling. This approach is useful, particularly in systems covering or interacting with domains other than fluid, e.g., mechanical or electrical domains. Hydraulic system modeling is often applied in these contexts [1]. This approach abstracts the system into a lumped one-dimensional dynamic system. Semiactive dampers are particularly apt candidates for this modeling approach. Semiactive damping technology [2] is increasingly applied in many industrial applications. Various conceptual approaches to semiactive vibration control have been studied in the past. The classical approach is represented by hydraulic semiactive dampers with controllable flow restrictors [2–5]. However, other alternative and novel approaches have been investigated recently, including dampers using the properties of electrorheological [6] and magnetorheological [7,8] fluids, dampers with combinations of magnetorheological fluids and elastomeric materials [9], Coulomb friction dampers [10], damping systems with magnetized particles [11], and colloidal dampers by using water-based ferrofluids [12]. The range of applications of these controllable devices spans early applications in car suspension systems [2], civil engineering applications [3,4], and aerospace vibration and damping augmentation systems [5,8–10,13]. The classical approach to semiactive hydraulic damping is studied here. This topic was discussed in theoretical terms in [14]. The general working context can be associated with the steady operation of rotating machinery [15] or helicopters [16,17]. The research presented in this paper is a continuation of the investigations

originally presented in [5,14,18]. The characteristic and novel aspect of the work presented here is the combined experimental–numerical approach to the study of the modified full-scale damper. The main contributions of this work, as perceived from the aerospace point of view, are related to the successful implementation, modeling, and correlation of the damper within a specified excitation framework. The wide range of topics associated with modeling, implementation, testing, simulation, and model-test correlation is discussed in this paper. This work was completed as a part of the Rotor Embedded Actuator Control Technology project, a Technology Strategy Board sponsored program funded by the Department for Business, Innovation, and Skills in the United Kingdom.

Section I of this paper surveys the area of semiactive damper research and places the current work in the wider context of previous research. Section II introduces general modeling topics with particular focus on the specifics of the modified hydraulic damper. The laboratory test configuration, the modified damper, and its mathematical model are described in Sec. III. The experiments and testing philosophy, based on periodic modulation of the damper flow restrictor, are presented in Sec. IV. Section IV.C presents a qualitative correlation study between the experimental data and the analytical model, as well as an analysis of the model performance achieved.

II. Modeling of the Semiactive Hydraulic Damper

A. Baseline Model of the Symmetric Hydraulic Damper

A class of hydraulic dampers with symmetric pistons is assumed in this work. Symmetric action of these devices is reflected in the nominally symmetric responses produced by the dampers during their forced excitation. The current investigation focuses on certain performance-related aspects of the damper operation and their reflection in the modeling techniques, aiming to capture the essential dynamic characteristics. The damper arrangement is presented in Fig. 1. As indicated in this figure, some functional aspects of damper design are not included in the model: most notably the initial damper pressurization, low-pressure protection mechanisms, and temperature variability. Figure 1a shows the general damper arrangement with two working pressure chambers, a piston, and a number of flow passages located between the two chambers. Piston-induced forced flow of the fluid through the available flowpaths leads to a pressure difference between two working chambers, and this difference is perceived as a motion-resisting force acting along the piston axis. The number of flow passages between the two working chambers represents the nominally available flow passages, covering both performance and operational aspects of damper use. Because of the specific nature of the present experimental work, this paper will use a model specialization corresponding to the situation indicated in Fig. 1b. This figure shows a damper with two flow passages, where one can be thought of as nominally present in the original damper design, while the second fluid passage is a modification introduced in the course of the current experimental activities.

Figure 1 provides a simplified schematic description of the main damper elements. This arrangement indicates that these systems can be seen as high-pressure closed-loop hydraulic systems operating in direct coupling with the mechanical domain, which provides the damper excitation. On account of this configuration, a low-order dynamic model of the damper in Fig. 1a will be constructed using hydraulic system theory [1]. This methodology enables the capture of the main characteristic modes of behavior of these systems such as flow induced nonlinearities, hysteretic behavior, elastic influences, and many others. The mathematical model of the general symmetric two-chamber damper setup described in Fig. 1a can be based on a single dynamic state: the pressure difference $\Delta p = p_1 - p_2$, where p_1 and p_2 are absolute homogeneous pressures in the two damper working chambers.

The model of the damper used here was introduced by Titurus and Lieven [14], who presented a derivation of the model alongside analytic investigations. The work presented in the current paper is a direct extension of the work presented in [14]. The model of the damper shown in Fig. 1a can be represented by a single non-autonomous differential equation

$$\frac{\mathrm{d}(\Delta p)}{\mathrm{d}t} = B_{0,\mathrm{eff}}\left(\frac{1}{V_1(y_P)} + \frac{1}{V_2(y_P)}\right) \times \left[A_P \frac{\mathrm{d}y_P}{\mathrm{d}t} - \sum_{j=1}^{N_F} Q_j(\Delta p)\right] \tag{1}$$

where $B_{0,\mathrm{eff}}$ is the constant effective bulk modulus of a hydraulic fluid, $V_1 = V_{0,1} - A_P y_P$ and $V_2 = V_{0,2} + A_P y_P$ are the volumes of the working chambers, $V_{0,1}$ and $V_{0,2}$ are the initial volumes of the working chambers, A_P is the wetted cross-sectional area of the symmetric piston, $y_P = y_P(t)$ is the piston displacement, N_F is the total number of fluid passages between the working chambers, and $\mathrm{d}(\circ)/\mathrm{d}t$ represents the time derivative or the rate of change of the corresponding quantity in the brackets. Finally, $Q_j = Q_j(\Delta p)$ represents the static pressure-flow characteristic, giving the volumetric flow rate between working chambers associated with the jth flowpath.

Model (1) represents a scalable alternative to the standard two-state hydraulic damper models (e.g., [3,4]) with reduced computational load and a more obvious link with the mechanical domain through the state of the model Δp. This arrangement is made possible due to the symmetric arrangement of the damper piston, seen in Fig. 1a. In the hydraulic domain, essential nonlinear aspects of the damper performance are retained such as hysteretic or nonideal damper behavior and nonlinear pressure-flow characteristics. Nonideal damper behavior, represented through its ability to store and release accumulated energy, is due to nonzero effective bulk modulus $B_{0,\mathrm{eff}}$. This quantity comprises a number of design and physical features related to the finite stiffness of the damper components, including the hydraulic fluid [19]. Nonlinear overall pressure-flow characteristics result from combination of the specific flowpath topology and the generally mixed laminar-turbulent flow conditions in these flowpaths [14]. The scalability of model (1) relates to the capability for its extension through inclusion of additional components such as relief valves [18]. In addition to the working chambers used for the modeling, the damper also possesses

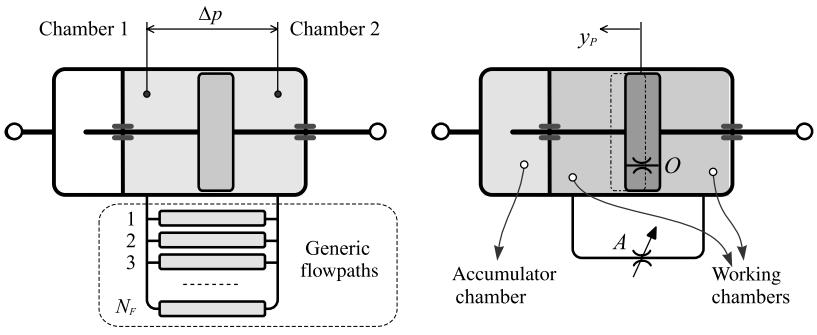

Fig. 1 Generic and two-branch semiactive hydraulic damper models: a) generic symmetric hydraulic damper with multiple flowpaths, and b) hydraulic damper with two parallel flowpaths (accumulator not modeled).

an accumulator to accommodate changes due to thermal expansion and fluid seepage losses and to establish a reference pressurization level to counter fluid compressibility and cavitation effects. A general outline of the working chambers and accumulator is given in Fig. 1b. However, the flow network associated with the accumulator is not shown; this flowpath is relatively restrictive and is not thought to make a significant contribution to the dynamics of interest here. As such, this part of the damper was omitted from the modeling.

B. Damper Model with Two Parallel Flowpaths

The specific damper setup used during experimental investigations can be modeled on the basis of Eq. (1). For the purposes of the current investigation, an existing damper with a single orifice, a pair of relief valves, and a full symmetric design was modified though its augmentation with an additional, controllable flowpath. The implementation of this modification is covered in more detail in Sec. III. The structural scheme of the modified damper is provided in Fig. 1b. This configuration represents a specialization of the model introduced in Eq. (1), and the new model can be written in the following form:

$$\frac{\mathrm{d}(\Delta p)}{\mathrm{d}t} = B_{0,\mathrm{eff}}\left(\frac{1}{V_1(y_P)} + \frac{1}{V_2(y_P)}\right) \times \left[A_P \frac{\mathrm{d}y_P}{\mathrm{d}t} - Q_O(\Delta p) - Q_A(\Delta p)\right] \tag{2}$$

where Q_O is the flow rate through the nominally available orifice, and Q_A is the flow rate through the newly introduced controllable, or active, flowpath.

Equation (2) can alternatively be written in a form that emphasizes the underlying relationships between different design elements of the damper. Dividing by the bulk modulus and the bracketed volume term, and performing minor rearrangements, this equation is as follows:

$$\beta_{0,\mathrm{eff}}\mathcal{V}(y_P)\Delta\dot{p} + Q_O(\Delta p) + Q_A(\Delta p) = A_P\dot{y}_P \tag{3}$$

where $\beta_{0,\mathrm{eff}} = 1/B_{0,\mathrm{eff}}$ is the effective compressibility of the hydraulic fluid, and $\mathcal{V}(y_P) = V_1V_2/(V_1 + V_2)$. The dynamic volumetric flow rate equilibrium between the terms in Eq. (3) can be reduced to a classical static equilibrium condition by assuming $\beta_{0,\mathrm{eff}} = 0$ (i.e., incompressible hydraulic fluid and rigid damper components) to give $Q_O + Q_A = Q_P$, where $Q_P = A_P\dot{y}_P$. This reduced formula and its more general analogs can be used for initial damper sizing and design tasks.

III. Theoretical and Practical Aspects of Damper Augmentation

A. Damper Modification Approach and Modeling Implications

In this section, the theoretical framework described above is put into context with the actual implementation of the damper modification. This modification augments the original passive damper with components enabling a semiactive mode of operation. This means that the damper retains its passive nature with respect to the mechanism of force generation, while the basic damper characteristics can be altered within a range determined by the nature of the damper modification. The modified damper therefore provides a realistic laboratory test platform allowing the assessment of a range of research and development questions, such as basic semiactive functionality, control investigations, design and sizing topics, failure mode scenario analysis, and broader simulation-oriented tasks. The research in this paper focuses on the hydraulic damper operating in a steady response mode with periodic modulations of the damping characteristics.

The existing physical damper infrastructure was exploited for the integration of the new controllable flowpath: the two existing hydraulic bleeding ports, linked with each of the working chambers, provided connection points for the additional flowpath. Furthermore, the newly added subsystem was designed such that it retained the refilling features of the damper. The controllable flowpath was built as a combination of a bespoke interface manifold and a standard industrial servovalve with four fluid ports and three specific spool positions (4×3 hydraulic servovalve) [20].

The in-house designed interface manifold, seen in Fig. 2, implemented the physical link between the two damper ports

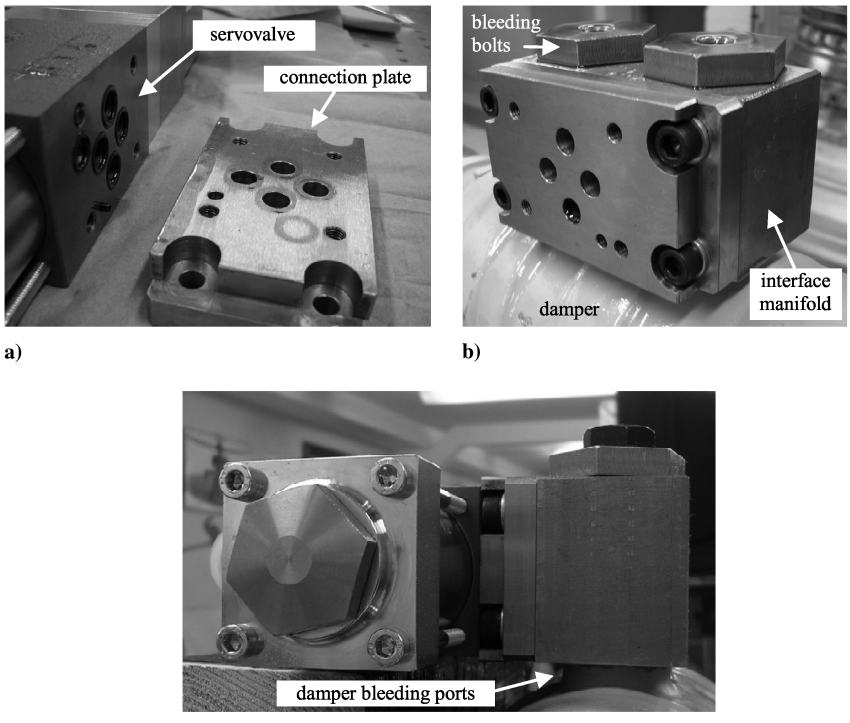

Fig. 2 Physical components of the modified hydraulic damper: a) connection plate with D636 servovalve, b) extension assembly with interface manifold and connection plate, and c) complete damper extension assembly.

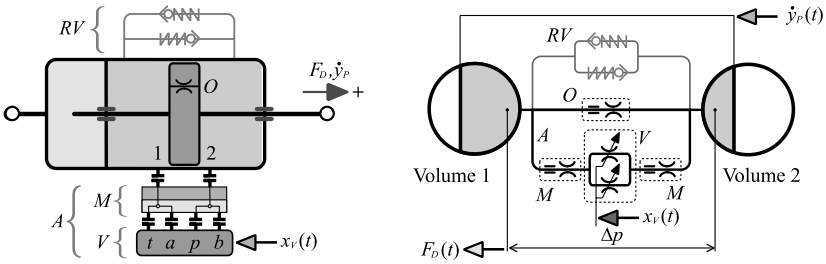

Fig. 3 Modified hydraulic damper: a) semiactive damper functionality, and b) hydraulic network with laminar and turbulent pressure loss elements.

(working chambers 1 and 2) and the four servovalve ports while converting the servovalve from a standard 4×3 operational mode into a 2–2 mode, i.e., two nominally identical orifices operating in parallel. A standard direct drive servovalve Moog D636 [20] was used as a readily available off-the-shelf component providing the functionality of a controllable orifice, with certain desirable features such as a fail-safe operation (converting the modified semiactive damper to its original passive operational regime on failure) and the presence of a spool position feedback control loop.

The damper modification depicted in this section provides a laboratory demonstrator with the required semiactive functionality. One constraint resulting from this approach is the limited extent of the geometric changes achievable by the active orifice with the available off-the-shelf solutions. Technical details regarding the chosen modification will be provided in the experimental part of the paper.

B. Complete Model of the Real Augmented Semiactive Hydraulic Damper

While previous sections presented a generic dynamic model of the hydraulic closed-loop two-chamber damper, this section will conclude the modified damper modeling with static pressure-flow characteristics of the specific damper topology. This part of the model will therefore deal with specific mathematical forms for the flow rate terms Q_O and Q_A.

Equally as in the case of the generic dynamic model of the damper, a lumped parameter approach is chosen for the static part of the model, which represents the flowpath connectivity and associated pressure loss mechanisms. Two modes of pressure loss mechanism are assumed throughout this paper: laminar and turbulent flows. Laminar flow and its associated pressure losses will be modeled via the linear relationship $\Delta p_L = C_L Q$, and similarly turbulent flow and its associated pressure losses will be modeled via the quadratic relationship $\Delta p_Q = C_Q Q|Q|$. In these formulas, C_L and C_Q are the pressure-flow coefficients for the laminar and the turbulent flow, respectively. These coefficients can be linked with the specific design and physical parameters of the hydraulic flowpath [19]. Furthermore, parallel and serial flowpath arrangements combined with the usual assumptions of mass (or volume) flow rate conservation will provide a suitable basis for static modeling.

A hydraulic network representing the topology of the modified damper is shown in Fig. 3. While Fig. 3b shows the complete hydraulic network with all constituent flowpaths and associated flow restrictors, Fig. 3a provides a basic representation of all the relevant flowpaths considered in the semiactive damper modeling, where O is the orifice; RV are the relief valves; M is the interface manifold; A is the active flowpath; and V is the servovalve with the labels t, a, p, and b representing the four servovalve hydraulic ports [20]). Figure 3b includes all the individual constituent elements, such as the interface manifold, the hydraulic servovalve, and the original orifice. In this figure, the flowpaths in the interface manifold are associated with both laminar (orifice symbol with straight lines) and turbulent (standard curved orifice symbol) pressure losses. The flow restrictors in the servovalve are associated only with turbulent pressure losses.

A serial arrangement of N_L discrete laminar and N_Q turbulent pressure loss components in the ith flowpath can be linked with the pressure difference induced by the flow through this flowpath in the form

$$\Delta p_i = \left(\sum_{j=1}^{N_L} C_{L,ij}\right) Q_i + \left(\sum_{k=1}^{N_Q} C_{Q,ik}\right) Q_i|Q_i| = C_{L,i} Q_i + C_{Q,i} Q_i|Q_i| \tag{4}$$

where $C_{L,ij}$ and $C_{Q,ik}$ are the pressure-flow coefficients due to the jth laminar and kth turbulent segments, respectively, in the lumped ith flowpath segments. These segment-specific loss coefficients combine into the total laminar $C_{L,i}$ and total turbulent $C_{Q,i}$ ith flowpath components. This formula allows the formulation of the inverse flow-pressure relationship in the following form:

$$Q_i = \text{sign}(\Delta p_i)(-C_{L,i} + (C_{L,i}^2 + 4C_{Q,i}|\Delta p_i|)^{1/2})/2C_{Q,i}$$

This process can be directly applied to the passive flowpath with the original orifice. The pressure-flow coefficients used in this case are $C_{L,O}$ and $C_{Q,O}$. The pressure differential for this branch Δp_O is assumed such that $\Delta p = \Delta p_O$. The augmented flowpath consists of the interface manifold and the hydraulic servovalve, and it is modeled as a serial–parallel combination of laminar and turbulent discrete pressure loss segments. The pressure difference in this branch is assumed to take a form consisting of the following contributions (Fig. 3):

$$\Delta p = \Delta p_A = \Delta p_{L,M} + \Delta p_{Q,M} + \Delta p_{Q,V} = C_{L,M} Q + (C_{Q,M} + C_{Q,V}^*(x_V))Q|Q| \tag{5}$$

where $\Delta p_{L,M}$, $\Delta p_{Q,M}$, and $\Delta p_{Q,V}$ are the increments of the total pressure difference corresponding to the laminar and turbulent flow-pressure losses in the interface manifold and turbulent flow-pressure losses in the servovalve, respectively; $C_{L,M}$ and $C_{Q,M}$ are the laminar and turbulent flow pressure-flow coefficients due to interface manifold. The coefficient $C_{Q,V}^* = (\frac{1}{4})C_{Q,V}(x_V)$ is the pressure-flow coefficient due to the assumed turbulent flow in the servovalve, where two nominally identical orifices are assumed to be operating in parallel. The pressure-flow coefficient for a single controllable flow subbranch $C_{Q,V}$ represents a single controllable element of the damper, where $C_{Q,V}(x_V) = \rho/(2C_{D,V}^2 A_V^2(x_V))$, $C_{D,V}$ is the discharge coefficient, x_V is the displacement of the servovalve's spool, and the relationship for the valve orifice area $A_V = A_V(x_V)$ can be represented by a lookup table or semiempirical relationship derived from dedicated experiments [21]. Finally, a new notation is introduced for the active flowpath, where $C_{L,A} = C_{L,M}$ and $C_{Q,A} = C_{Q,M} + C_{Q,V}^*(x_V)$.

Considering the two flow branches according to Fig. 3 and the theoretical development linked with Eqs. (4) and (5), the terms for Q_O and Q_A in Eq. (3) can be substituted, resulting in a final model of the modified damper

$$\beta_{0,\text{eff}}\mathcal{V}(y_P)\Delta\dot{p} + \text{sign}(\Delta p)\left(\frac{-C_{L,O} + \sqrt{C_{L,O}^2 + 4C_{Q,O}|\Delta p|}}{2C_{Q,O}}\right.$$

$$\left. + \frac{-C_{L,A} + \sqrt{C_{L,A}^2 + 4C_{Q,A}(x_V)|\Delta p|}}{2C_{Q,A}(x_V)}\right) = A_P\dot{y}_P \tag{6}$$

This equation will be used with experimentally determined coefficients $C_{L,O}$, $C_{Q,O}$, and $C_{L,A}$. In the composite coefficient $C_{Q,A} = C_{Q,M} + C^*_{Q,V}(x_V)$, the part $C^*_{Q,V} = (\frac{1}{4})C_{Q,V}(x_V)$ will be used with parameter $C_{D,V} = 0.65$ and the lookup table $A_V = A_V(x_V)$ as provided by the manufacturer of the servovalve [20]. The numerical solution of this equation implemented in the MATLAB® programming environment [22] with the variable-step-length numerical integration algorithm implemented in the ODE45 function will be performed with initial conditions $\Delta p = 0$. Excitation of this equation $\dot{y}_P$ and the variable nature of the coefficient $\mathcal{V}(y_P)$ will be determined from the experimental conditions measured by the integrated hydraulic actuator instrumentation.

C. Test Setup and Nominal Performance of the Modified Damper

While it is not the focus of this paper to investigate the full, nominal semiactive behavior of the modified hydraulic damper, this section will provide a brief outline of its performance. To achieve this, selected characteristic cases are presented in Fig. 4. The three cases cover regimes with full-, partial-, and no-relief valve contribution to the damper's behavior, achieved using identical excitation conditions and varying static active orifice openings. The relief valves and their associated functionality are not a subject of the current research; therefore, they will be included in this section only for the sake of completeness. In Fig. 4, two standard damper characteristics are provided: 1) piston displacement and damper force, or simply displacement-force characteristics; and 2) piston velocity and damper force, or simply velocity-force characteristics. The data presented in these figures are normalized with respect to the maximum forces, displacements, and velocities due to their commercial sensitivity.

Figure 4 shows a selection of five different tests to demonstrate a number of different behaviors of the damper. A range of servovalve openings is used with two distinct excitation waveforms and test methodologies. Thus, the domains of semiactive operation and relief valve activation, and the effects of compressibility are observable and mutually comparable. Progressive opening of the controllable flowpath allows increasing flow rate capacities with reduced pressure differentials. In this manner, the damping mode with significant relief valve activity can be transformed into a regime with marginal or no relief valve presence. Opening of the controllable flowpath reduces the force levels from those originally determined by strong relief valve hydromechanical interactions (e.g., spring precompression levels) to those fully determined by the hydraulic system dynamics. The velocity-force characteristic domain provides a good illustration of most of the factors limiting the damper performance. The nominal or idealized nature of velocity sensitive dampers can be illustrated by the line characteristics in this domain. Nonidealized or more complex damper behavior results in hysteretic or closed-loop characteristics in this domain. Semiactive functionality extends these characteristics into regions typically localized in the first and the third quadrants of the velocity-force domains. The shape of these regions is, in the present case, determined by 1) a relatively shallow low-velocity quadratic-shaped boundary for the case with the fully open controllable orifice $Q_{A,\max}$; 2) a relatively steep low-velocity quadratic-shaped boundary for the case with the fully closed orifice $Q_{A,\min} \to 0$; and 3) a relatively shallow, generally quadratic upper boundary. Finally, high-velocity and maximum-displacement boundaries can be postulated based on damper design and maximum load considerations.

Only a subset of generally reachable velocity-force regions will be accessed in the following studies. The test regimes will be proposed such that no relief valve action will be induced. The topology of the current damper modification allows for fail-safe damper operation, where due to the presence of a centering spring element in the servovalve, failure in the control element leads to $Q_{A,\min} \to 0$. This

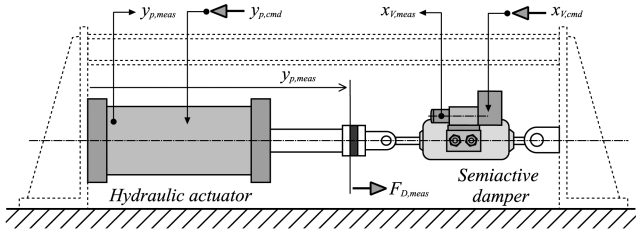

a)

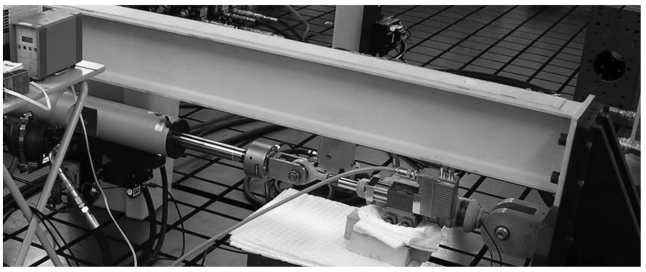

b)

Fig. 5 Test rig for experimental studies with modified semiactive hydraulic damper: a) basic test rig configuration and signals, and b) test rig during experiments.

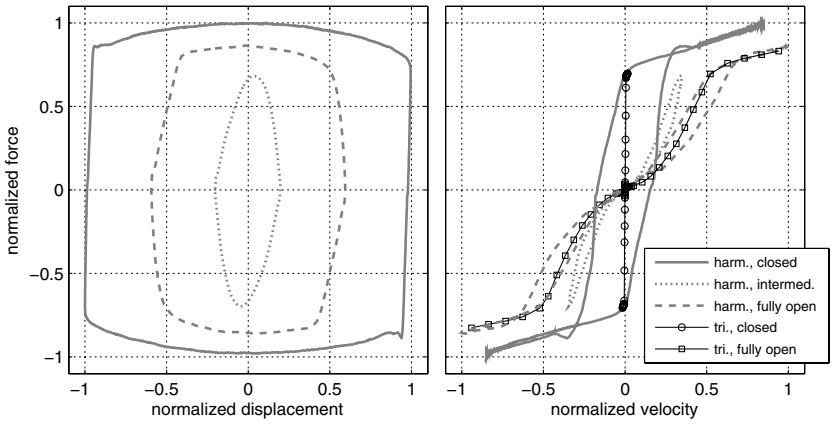

Fig. 4 Example of the performance of the modified damper. Three selected test regimes indicated in the legend: "harm." represents harmonic piston excitation, and "tri." represents triangular piston excitation [19].

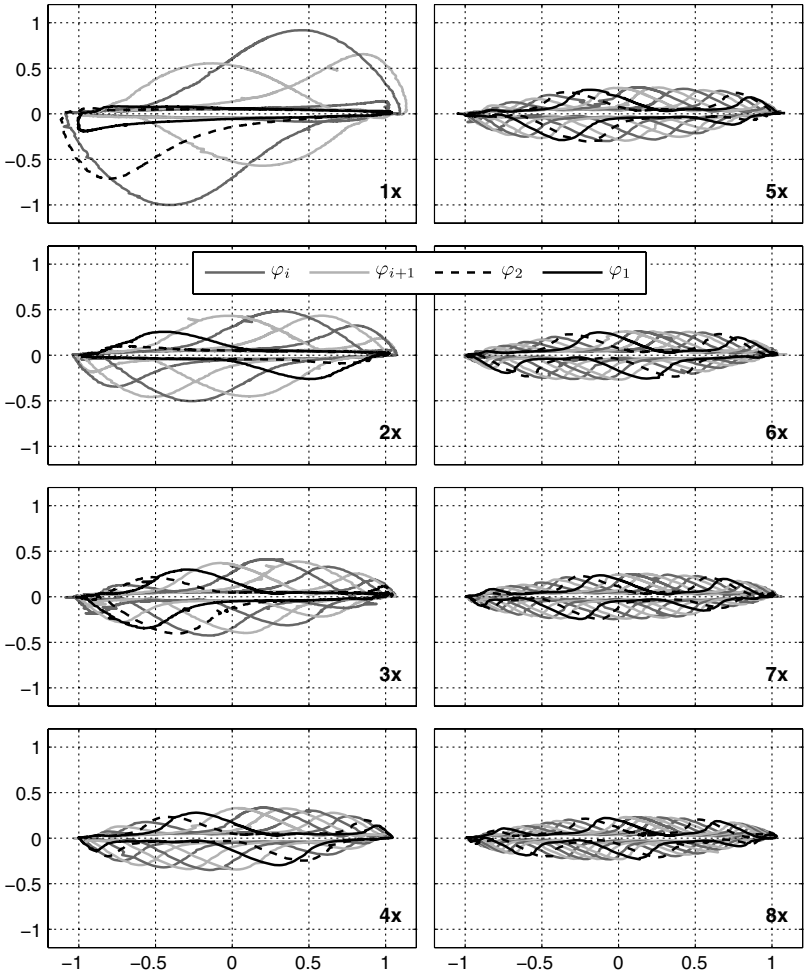

Fig. 6 Piston displacement [mm] vs damper force (normalized) for 50 ± 45% x_V modulation and {1–8}x modulation frequencies.

case therefore brings the modified damper into its original fully passive state, which is generally a functionally desirable feature of a semiactive damper.

IV. Experimental Results

A. Test Conditions for Damper Tests with Periodic Parameter Modulation

The investigation presented in [14] provided a theoretical treatment of a semiactive hydraulic damper in a periodic working environment. The operating conditions used in that research will be used in this work: now, on the real modified semiactive damper. The experimental setup applied here is described in Fig. 5. A detailed description of the constituent experimental components is provided in [19].

The main physical components of the test system are a linear hydraulic actuator with an Instron control system, a modified hydraulic damper linked to a dSpace test control system, and a high-stiffness test rig frame. Signals generated and recorded during the test cases include the force signal measured by a load cell located between the damper and the actuator; the actuator piston displacement via its own integrated linear variable differential transformer (LVDT); and the servovalve augmentation's spool displacement via its integrated LVDT. The remaining two recorded signals are the command signals for the actuator and spool displacements. This configuration is shown in Fig. 5.

To be able to perform a numerical simulation of the investigated system, the pressure-flow coefficients had to be estimated in a dedicated identification study. As this study, consisting of specific tests and calculations, is out of the scope of this paper, only the resulting estimated coefficients are provided later in Sec. IV.C, Table 1. These coefficients will be used with model (6). During experiments, the damper is considered to be a system with two controlled inputs; piston displacement $y_P(t)$ and servovalve spool displacement $x_V(t)$; and one observed response, damper force $F_D(t)$. The fourth and fifth measured signals are the command signals: $y_{P,\mathrm{cmd}}(t)$ for prescribed piston displacement and $x_{V,\mathrm{cmd}}(t)$ for prescribed servovalve displacement.

Experiments were designed to enable exploration of the semiactive periodic damper performance for operationally relevant conditions. To retain periodic operation of the damper, both damper inputs were specified as harmonic command signals. The first input was kept invariant during individual tests, and it effectively represented a reference harmonic piston displacement $y_P(t) = A_P \sin(2\pi f_{\mathrm{ref}} t)$, where $A_P = 1$ mm, and $f_{\mathrm{ref}} = 3.5$ Hz. The resulting prescribed peak piston velocity was thus $\dot{y}_{P,\max} = 21.99$ mm/s. The second harmonic input applied to the servovalve represented the prescribed spool displacement $x_V(t)$. The harmonic servovalve inputs were specified as follows:

$$x_V(t) = x_{V,\max}(A_{V,0} + A_{V,1} \sin(\omega_j t + \varphi_k)) \tag{7}$$

where $A_{V,0} = 0.5$, $A_{V,1} = 0.45$, and $x_{V,\max} = 0.5$ mm; the frequency is $\omega_j = j2\pi f_{\mathrm{ref}}$; and the phase difference is $\varphi_k = 2\pi(k-1)/8$. The modulation frequency range, identified by the index j, is chosen to cover the frequencies that are relevant for potential future vibration control applications [5,16,17]. Indices j and k were specified as follows:

$$j, k \in \{1, 2, 3, 4, 5, 6, 7, 8\} \tag{8}$$

All combinations of the test frequencies and relative phase differences characterized by the index pairs $\{j, k\}$ constituted 84 test cases. Experimental results are documented in the next section. In addition, three selected test cases will be used for a correlation study

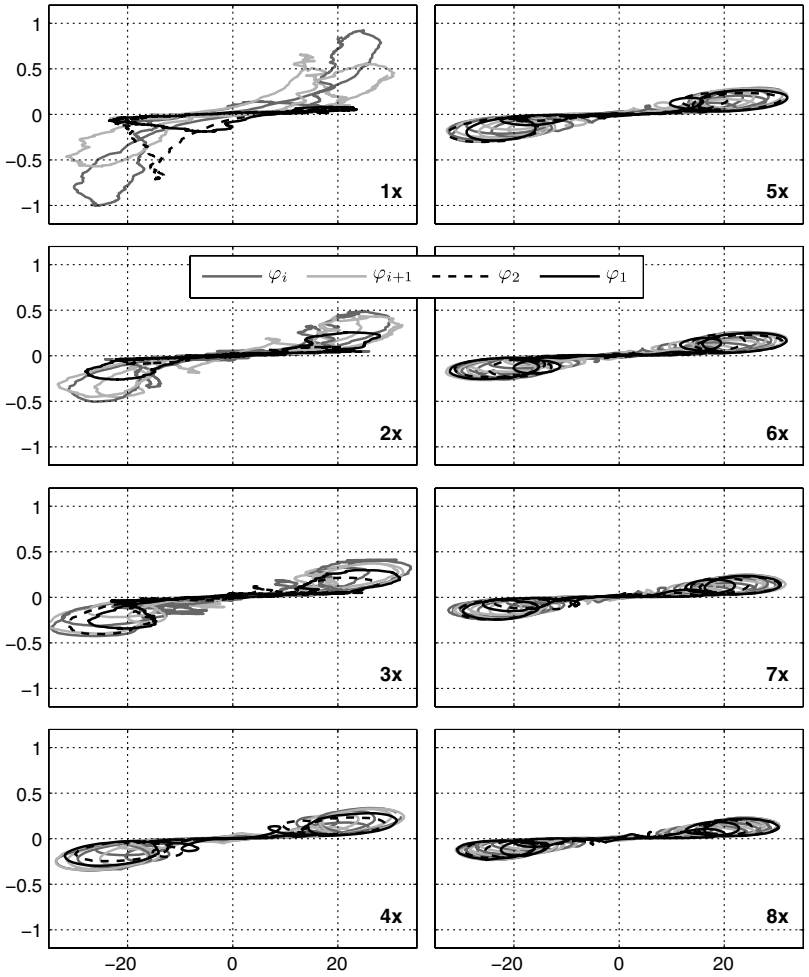

Fig. 7 Piston velocity [mm/s] vs damper force (normalized) for 50 ± 45% x_V modulation and {1–8}x modulation frequencies.

with the corresponding simulated results. In this study, the measured periodic responses will be used to provide an analytical representation of the excitation signal $y_P(t)$, which will then be used to drive the numerical simulations.

B. Periodic Excitation Tests and Test Postprocessing

As in Fig. 4, the behavior of the damper will be observed in the displacement-force and velocity-force domains. A single pair $\{j, k\}$ will be further expanded and numerically processed to provide an alternative view on the effect of harmonic flow perturbation for the case of a periodically operated semiactive damper.

In the following analysis, Figs. 6 and 7 show measured data providing a complete overview of the results of the experimental study described in the previous section. Figure 6 shows displacement-force characteristics, while Fig. 7 presents velocity-force characteristics. Each figure consists of subplots corresponding to the index j, i.e., the servovalve modulation frequency, denoted as jx in these figures. Each subplot contains all the cases corresponding to the index k, i.e., the phase differences. Consequently, a complete range of variations in baseline damper characteristics is covered, providing information about the operational envelope and the influence of modulation frequency on the semiactive periodic operation of the damper. Measured data on the horizontal axes are presented in their unscaled form in the corresponding physical units: piston displacement y_P (in millimeters) and piston velocity (in millimeters per second). Because of their commercial sensitivity, the vertical axes in both figures show damper forces normalized with respect to the maximum force magnitude measured in the regime with $\omega = \omega_1$, denoted 1x in Figs. 6 and 7.

The two shades of gray are used alternately to improve the distinction between the eight phase-based consecutive loops in each subplot of Figs. 6 and 7. While these figures do not allow detailed study of the features present in the characteristics, they can be used to observe global patterns across phase differences and increasing frequency of flow restrictor modulations. Progressive increases in relative phase difference between y_P and x_V establish a pattern in the distribution of the force peaks for which the value depends on modulation frequency ω_j. At most, j force peaks should be present in the measured characteristics. However, this number of peaks may not be generally observable due to the near or exact timing concurrency of $\min(x_V)$ with $\dot{y}_P = 0$. This will be demonstrated in one of the selected measured data sets that follow. It can be seen in both Figs. 6 and 7 that increasing the frequency of the flow restrictor modulation results in a reduction of the peak force levels. This effect is a reflection of the increasingly unsteady flow conditions assembled in the time domain in a periodic manner and constituting the resulting periodic response of the damper. Reduced flow transition times corresponding to higher modulation frequencies lead to the development of lower pressure differentials and damper forces.

In the case of Fig. 7, the raw piston displacement signals were processed with Savitzky–Golay polynomial smoothing and differentiation filters as implemented in MATLAB [22]. This implementation was used to provide differentiation filters to estimate the piston velocity signals with a filter polynomial order of three and a frame size of 31 samples (as contrasted with the signal sampling frequency of 1000 Hz).

Owing to its causal working principles, the characteristics of the semiactive damper predominantly occupy subdomains located in the first and third quadrants of the velocity-force domain, i.e., $F_D \dot{y}_P \geq 0$. This correlates with the passive mechanism of damper force generation, which relies on induced fluid flow resulting from externally forced changes in the working chamber geometry. However, Fig. 7 also indicates the presence of damper force

responses in the second and fourth quadrants of the velocity-force domain, i.e., $F_D\dot{y}_P < 0$. These effects are usually associated with the effective compressibility of the fluid [1], a quantity which encompasses the fluid compressibility, entrapped air contamination, chamber compliance, and damper attachment stiffness. An almost fully open regime during harmonic modulation, that of a 95% open servovalve, causes all the characteristics in Fig. 7 to reach the lower achievable force boundary defined for the semiactive damper authority, as indicated in Fig. 4. The higher limit of the force envelope, however, changes between different cases of modulation frequency ω_j due to the transient dynamics of the process. In contrast with Fig. 6, velocity-force loops in Fig. 7 do not provide obvious and visually observable patterns. This is caused by the high density of the changes located in relatively small velocity-force subdomains and by the distortion of the reference harmonic piston velocity signal. The reference signal distortion is caused by the local test rig controller's inability to ensure accurate tracking of the commanded harmonic signal in an environment with a rate-dependent semiactive damper device. This will be illustrated in the following section.

The results summarized in Fig. 6 are further processed to express the dissipative nature of the damper, induced through different perturbation regimes $\{j, k\}$. The area enclosed by the displacement-force curves is characteristic of the work done by the actuator $W_{\{j,k\}}$ on the damper in one test period $T_{\text{ref}} = 1/f_{\text{ref}}$. The results for all the modulation combinations are summarized in Fig. 8.

Each curve in this plot describes a case of a single modulation frequency ω_j, and constituent points of these lines correspond to the different relative phase differences φ_k in Eq. (7). In the test case with frequency ω_1, the work $W_{\{1,:\}}$ changes in the range $(1.77, 9.01)J$, while in the case with ω_8, the work is $W_{\{8,:\}} \in (2.43, 2.50)J$. In the case with ω_3, later used for more detailed studies, the interval is $W_{\{3,:\}} \in (3.11, 3.49)J$. These results indicate strong dependency of $W_{\{j,k\}}$ on the relative phase differences φ_k as well as degradation in the amount and in the extent of $W_{\{j,k\}}$ variability with increasing modulation frequency ω_j. These effects are caused by varying flow restrictor opening and closing times and changing the relative position of the $\min(x_V)$ with $\dot{y}_P = 0$.

The foregoing, in effect global, analysis of the dissipative damper properties is now complemented with an in-depth frequency domain analysis of the damper force responses, given for a single frequency modulation ω_j and a range of phase differences $\varphi_k = 2\pi(k-1)/60$, $j = 3, k \in \{1, \ldots, 60\}$. The results of this analysis are shown in Fig. 9, giving the Fourier breakdown of the piston force response for each φ_k. Whereas the individual curves in Fig. 8 correspond to different damper modulation frequencies ω_j, those in Fig. 9 represent the different frequency components ω_l of the force response, obtained from a single modulation frequency ω_j. Denoted by different marker styles, the response components are shown with sine and cosine components on the ordinate and abscissa, respectively, with the filled circle markers indicating the case $\varphi_1 = 0$. The discrete time series are processed such that

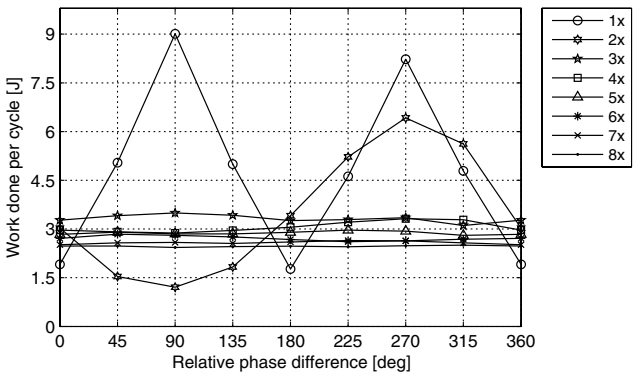

Fig. 8 Mechanical work done per single test cycle for all 64 test cases: {1–8}x represent the servovalve modulation frequency as the integer multiple of the reference (piston) frequency.

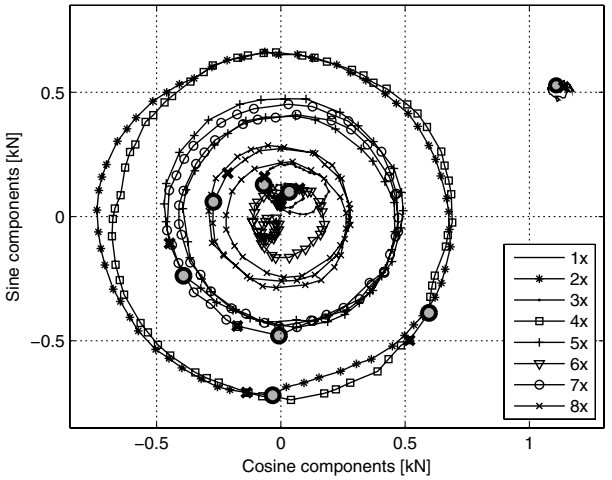

Fig. 9 Fourier analysis of the measured damper forces during the harmonic servovalve perturbation exercise for all harmonic inputs $\{3, k\}$, where $k = 1, 2, \ldots, 60$. The legend identifies the individual harmonic components.

$$F_{D,\{j,k\}}(t_i) = F_{D,\{j,k\},0} + \sum_{l=1}^{N_{FA}} (F_{D,\{j,k\},C,l}\cos(l2\pi f_{\text{ref}} t_i) + F_{D,\{j,k\},S,l}\sin(l2\pi f_{\text{ref}} t_i)) \tag{9}$$

where $A_l = F_{D,\{j,k\},C,l}$ and $B_l = F_{D,\{j,k\},S,l}$ are the Fourier cosine and sine coefficients, respectively, of the N_{FA} components of the Fourier series decomposition, obtained from analyses on single-period blocks of the damper forces $F_{D,\{j,k\}}(t)$, where $t \in [t_I, t_I + T_{\text{ref}}]$, and t_I is the arbitrary reference time point. These coefficients are computed in a linear least-squares process based on the linear functional representation shown in Eq. (9).

While Fig. 8 provides a global assessment of the changes in dissipative properties of the damper due to both frequency and phase changes, Fig. 9 focuses on the force changes induced by a specific periodic modulation where $j = 3$, this time using a refined spectrum of relative phases to improve the clarity of the presentation. The points in Fig. 9 can be interpreted as the sensitivity characteristics of the semiactive damper system, indicating the extent and the character of the force changes induced by this modulation frequency. This is something that is interesting in the context of existing active vibration control algorithms [17], which rely on measurements of such sensitivities for their operation. This figure thus provides closer insight into possible mechanisms of semiactive damper control for vibration reduction in periodic working environments such as helicopters in steady flight conditions [18]. Variation of the active orifice, both on the amplitude and phase levels, possibly in the form of multiharmonic control inputs, can be used to provide optimal adjustments to meet given reference response damper characteristics.

It can be observed in the figure that a given damper modulation frequency (in this case, $j = 3$) strongly influences pairs of Fourier components with frequencies ω_r, where $r = (I \times j) \pm 1$ and I is a positive integer. In contrast, only minor influences can be observed for the components with frequencies ω_s, where $s = I \times j$. This experimental observation correlates well with a similar, theoretical configuration investigated in [14]. In that case, an identical modulation scenario applied to the model of a damper with a comparable topology resulted in dominant, or sensitive, responses at the Fourier coefficients with frequencies $r = (1 \times 3) \pm 1 \equiv \{2, 4\}$. Similarly, the current configuration indicates the highest sensitivity for the components at the same two frequencies $r \in \{2, 4\}$. The higher-order components in the present study, where $I > 1$, show increased sensitivities when compared with those from the previous work, and this can be directly attributed to a increased nonlinearity in the relationship between the servovalve spool displacement and the associated pressure loss characteristics of the flowpath.

Table 1 Pressure-flow coefficients of the semiactive hydraulic damper

Coefficient	Units	Value
$C_{L,O}$	$\mathrm{kg \cdot m^{-4} \cdot s^{-1}}$	3.6970×10^{10}
$C_{Q,O}$	$\mathrm{kg \cdot m^{-7}}$	4.5297×10^{16}
$C_{L,M}$	$\mathrm{kg \cdot m^{-4} \cdot s^{-1}}$	4.7006×10^{8}
$C_{Q,M}$	$\mathrm{kg \cdot m^{-7}}$	1.5954×10^{12}
$C^*_{Q,V}(x_V)$	$\mathrm{kg \cdot m^{-7}}$	Lookup table [20].

C. Correlation Between Tests and Analytical Results

This section provides a representative correlation study between the experimental results presented in the foregoing parts of the paper and the predictions based on mathematical model (6). The intention is to demonstrate the predictive capabilities of a simple one-equation reduced-order model of the semiactive damper [Eq. (6)] assuming an operational mode without relief valve activation. Also, some associated test-related problems will be highlighted, as well as the approach chosen in this work to overcome them.

Equation (6) is used with parameters identified experimentally with the help of a combination of standard and novel experimental techniques. The coefficients $C_{L,O}$ and $C_{Q,O}$ were identified with triangular excitation providing piecewise constant piston velocities and leading to quasi-steady flow conditions in the damper [19]. This approach enabled an experimental focus on the investigated physical behavior, i.e., composite hydraulic losses occurring during orifice-only flow regime. The coefficients $C_{L,M}$ and $C_{Q,M}$ were identified assuming knowledge of the damper topology and the associated coefficients $C_{L,O}$, $C_{Q,O}$, and $C^*_{Q,V}(x_V)$. The coefficient $C^*_{Q,V}(x_V)$ was determined from the servovalve's pressure-flow characteristics [20]. The identification process of the coefficients $C_{L,M}$ and $C_{Q,M}$ was based on an experimental design with harmonic piston excitation. The values identified for the pressure-flow coefficients are summarized in Table 1.

The damper as modeled is, in effect, a rate-dependent device; moreover, the considerable hydraulic resistance variations exhibited by the damper during periodic modulations increase the demands on the hardware controller in attempting to apply simple harmonic piston displacements. The nonadaptive proportional-integral-derivative-lag controller available with the Instron test control system was not capable of ensuring a consistent quality of applied piston displacements throughout the full range of tests, resulting in higher harmonic distortions of the applied reference signal. The distorted piston displacement signal shown in Fig. 10 corresponds to the case $\{4, 2\}$. It is important, for the purposes of correlation studies, to establish comparable conditions for the generation of both data sets: experimental and numerical. The approach chosen in this paper is to introduce a simulated piston excitation that corresponds to the actual recorded experimental piston displacements. Figure 10 indicates part of that process. The original centered time domain piston displacement signal is decomposed into single-period blocks, and a number of these are used to determine the mean piston displacement signal. In Fig. 10, the thick dark gray background lines represent a number of individual one-period blocks overlaid, while the thick light gray line represents the mean piston displacement signal. The one-period mean signal is then decomposed into its constituent harmonic components using a finite Fourier series representation similar to Eq. (9). In all three cases presented below, the first 30 harmonics were chosen. An example of a synthesized piston excitation signal is shown in Fig. 10 as a thin black line.

Figures 11–13, provide three examples of the correlation between experimental and numerical results. The format selected for the presentation uses the standard damper displacement-force and velocity-force characteristics. The two signals demonstrated in each

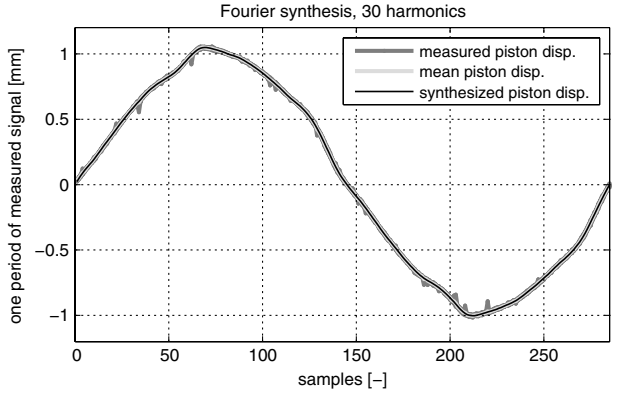

Fig. 10 Piston excitation signal (thin black line) synthesized by means of Fourier analysis of the mean piston displacement (light gray line), computed from the raw measured piston displacement signals (dark gray lines).

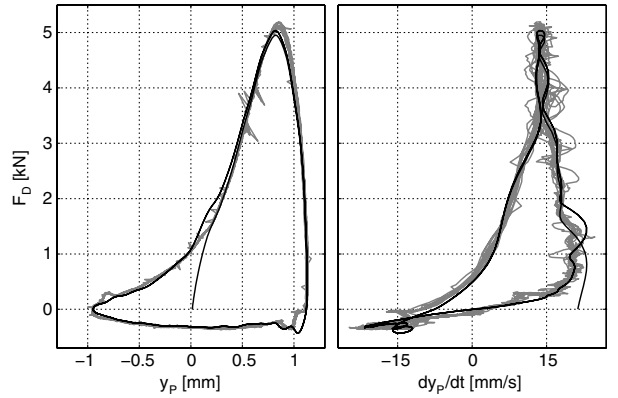

Fig. 11 Correlation study with modulation frequency ω_1 and phase difference of 225 deg, $\{j, k\} = \{1, 6\}$.

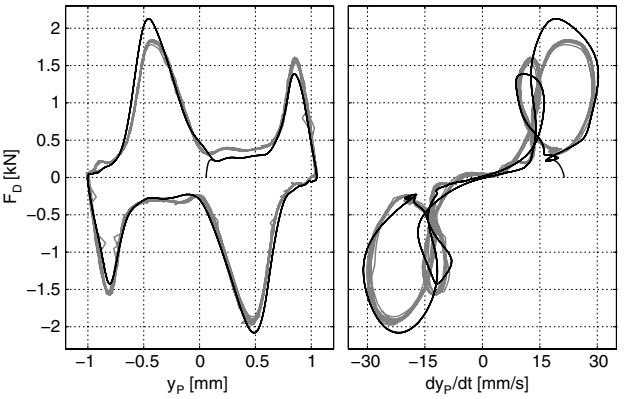

Fig. 12 Correlation study with modulation frequency ω_4 and phase difference of 45 deg, $\{j, k\} = \{4, 2\}$.

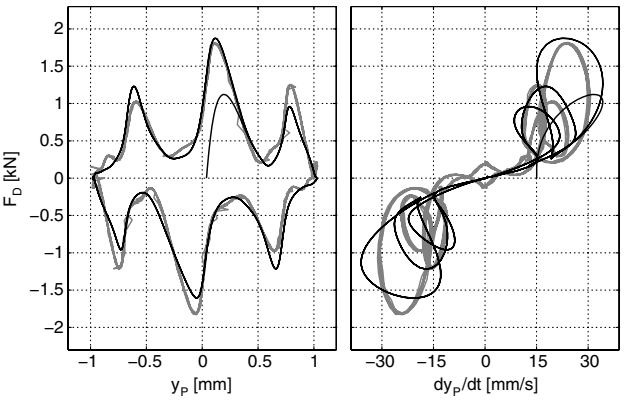

Fig. 13 Correlation study with modulation frequency ω_8 and phase difference of 315 deg, $\{j, k\} = \{8, 8\}$.

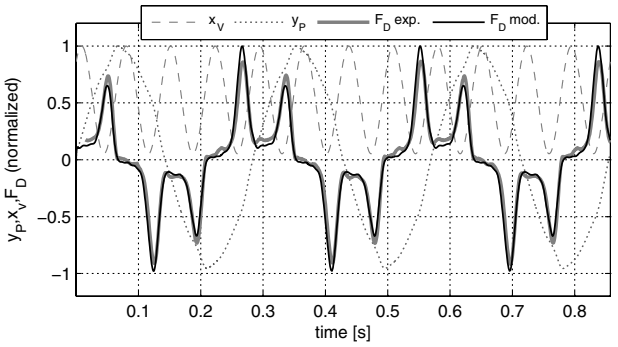

Fig. 14 Time domain results of the correlation study with modulation frequency ω_4 and phase difference of 45 deg, $\{j, k\} = \{4, 2\}$. All quantities are normalized to facilitate mutual comparisons.

plot are the recorded experimental signals (gray lines) and the simulated damper responses (black lines) based on the Fourier synthesized piston excitation.

These figures compare selected examples of the measured and calculated damper characteristic loops. They document that the single-state reduced-order model of the semiactive hydraulic damper [Eq. (6)] can capture important qualitative aspects of damper response. These are primarily force pulses that result from specific phase and frequency composition of the two signals: the piston velocity $\dot{y}_P$ and the spool displacement x_V. The effect of the mutual coupling of these two signals is also illustrated in Fig. 14 in the time domain after achieving steady periodic responses. In this figure, the black line represents the damper force predictions and these are compared here with the measured damper forces represented by the thick gray lines. The figure also shows two measured damper inputs, the piston and spool displacements, both represented by the thin gray lines.

Moreover, as it is possible to see from Figs. 11–14, this model of the damper is capable of providing realistic predictions of the response force levels despite the considerable degree of simplification. This ability to provide good indications of achievable performance with the semiactive damper in this operational regime is a result of the physics-based nature of this model. This model therefore can be considered as suitable candidate for further development studies or performance analyses.

Two areas for further improvement of model (6) are both linked with the current compressibility model and the potential for the existence of either manufacturing or built-in asymmetries. Within the context of the available model structure, the asymmetry modeling could be improved by the introduction of flow-direction-dependent pressure-flow coefficients for all the modeled flowpaths. Improvements in the area of compressibility modeling, however, would require a departure from the current model structure, which employs only one dynamic state: the differential pressure. More advanced models of compressibility require the introduction of absolute pressure states.

V. Conclusions

This paper provides a summary overview of selected activities in the development of a semiactive hydraulic damper demonstrator. The semiactive damper was implemented by augmenting an existing hydraulic damper, used in production helicopters, with a new parallel controllable flowpath. This approach allowed a fast implementation of the concept in the realistic context of a production component. The specific periodic operational context of this modified component has been considered here due to its relevance to its possible future applications. The experimental activities presented also reflect upon this fact. The structural modification of the nominally passive damper was achieved through introduction of an interface assembly and a standard industrial servovalve. This modification, in combination with the original damper parameters, allowed the functional exploitation of the orifice control in the added flowpath for semiactive damper operation. The studies in this paper are limited to the operation of this modified damper without activation of the relief valves.

A single-state dynamic model of the damper has been presented based on hydraulic system modeling concepts. This model considers both compressibility effects in the system and the combined laminar–turbulent nature of the fluid flow in real conditions. Key parameters of the model were estimated from a set of dedicated identification experiments. The achieved performance of the semiactive damper features realistic limitations such as limited servovalve based orifice changes. A set of tests has been designed to allow systematic mapping of the damper's performance; this set comprises 64 tests covering eight cases of servovalve modulation frequency, each case with eight cases of phase difference between the piston excitation and servovalve modulation signals. Systematic test organization creates a suitable context to observe patterns in the measured damper responses. These are already apparent when examining the raw measured data for the case of each modulation frequency or, alternatively, further postprocessing can be applied to gain a more detailed understanding of the actual functional mechanisms behind the observed results. The first postprocessing exercise looked at the changes in the amounts of dissipated energies induced purely due to changes in the relative phase differences between two damper input signals. This exercise showed that significant variations in energy dissipation can be achieved for frequencies close to the reference piston excitation frequency, while this process progressively becomes inefficient for increasing modulation frequencies. The second postprocessing exercise considered the magnitude, frequency, and phase variations in the damper force responses induced via identical modulation mechanisms. Significant phase changes can be observed at selected frequencies related to the frequency content of both input signals. In the case of $3R$ servovalve modulation, major changes were observed at $2R$ and $4R$ frequencies.

The sensitivity of this process, within the experimental and operational contexts provided, points toward the useful application of this configuration via selective modulation of the semiactive damper with specific harmonic or more complex control signals. The present study provides an experimental confirmation of semiactive damper operational principles in a periodic working environment, and it documents the ability to create simple predictive physics-based models of sufficient quality for more complex simulation architectures, such as comprehensive helicopter aeroelastic performance studies with an objective of active or semiactive vibration control.

Acknowledgments

This work was supported by the United Kingdom Technology Strategy Board and AgustaWestland Helicopters through the Rotor Embedded Actuator Control Technology project. The authors gratefully acknowledge the support of AgustaWestland: in particular, the technical contributions of Ross Hilditch and Simon Stacey.

References

[1] Merritt, H. E., *Hydraulic Control Systems*, Wiley , New York, 1967, Chaps. 2, 3, 5.

[2] Karnopp, D., "Design Principles for Vibration Control Systems Using Semi-Active Dampers," *Journal of Dynamic Systems, Measurement, and Control*, Vol. 112, No. 3, Sept. 1990, pp. 448–455. doi:10.1115/1.2896163

[3] Patten, W. N., Mo, C., Kuehn, J., and Lee, J., "A Primer on Design of Semiactive Vibration Absorbers (SAVA)," *Journal of Engineering Mechanics*, Vol. 124, No. 1, Jan. 1998, pp. 61–68. doi:10.1061/(ASCE)0733-9399(1998)124:1(61)

[4] Symans, M. D., and Constantinou, M. C., "Experimental Testing and Analytical Modelling of Semi-Active Fluid Dampers for Seismic Protection," *Journal of Intelligent Material Systems and Structures*, Vol. 8, No. 8, Aug. 1997, pp. 644–657. doi:10.1177/1045389X9700800802

[5] Anusonti-Inthra, P., and Gandhi, F., "Reduction of Helicopter Vibration Through Cyclic Control of Variable Orifice Dampers," *The Aeronautical Journal*, Vol. 107, No. 1077, Nov. 2003, pp. 657–672.

[6] Honga, S. R., Choia, S. B., Choib,, and Wereley, N. M., "A Hydro-Mechanical Model for Hysteretic Damping Force Prediction of ER

Damper: Experimental Verification," *Journal of Sound and Vibration*, Vol. 285, Nos. 4–5, Aug. 2005, pp. 1180–1188. doi:10.1016/j.jsv.2004.10.031

[7] Kwok, N. M., Ha, Q. P., Nguyen, T. H., Li, J., and Samali, B., "A Novel Hysteretic Model for Magnetorheological Fluid Dampers and Parameter Identification Using Particle Swarm Optimization," *Sensors and Actuators A: Physical, Vol. 89, Nos. 1-2*, Vol. 132, No. 2, Nov. 2006, pp. 441–451. doi:10.1016/j.sna.2006.03.015

[8] Batterbee, D. C., Sims, N. D., Stanway, R., and Wolejsza, Z., "Magnetorheological Landing Gear: 1. A Design Methodology," *Smart Materials and Structures*, Vol. 16, No. 6, Dec. 2007, pp. 2429–2440. doi:10.1088/0964-1726/16/6/046

[9] Hu, W., Wereley, N. M., Chemouni, L., and Chen, P. C., "Semi-Active Linear Stroke Magnetorheological Fluid-Elastic Helicopter Lag Damper," *Journal of Guidance, Control, and Dynamics*, Vol. 30, No. 2, 2007, pp. 565–575. doi:10.2514/1.24033

[10] Bauchau, O. A., Van Weddingen, Y., and Agarwal, S., "Semiactive Coulomb Friction Lead–Lag Dampers," *Journal of the American Helicopter Society*, Vol. 55, No. 1, 2010, Paper 12005. doi: 10.4050/JAHS.55.012005

[11] Shah, B. M., Nudell, J. J., Kao, K. R., Keer, L. M., Wang, Q. J., and Zhou, K., "Semi-Active Particle-Based Damping Systems Controlled by Magnetic Fields," *Journal of Sound and Vibration*, Vol. 330, No. 2, Jan. 2011, pp. 155–360. doi:10.1016/j.jsv.2010.09.005

[12] Zhou, G. Y., and Sun, L. Z., "Smart Colloidal Dampers with On-Demand Controllable Damping Capability," *Smart Materials and Structures*, Vol. 17, No. 5, 2008, pp. 1–11. doi:10.1088/0964-1726/17/5/055023

[13] Zhao, Y., Choi, Y.-T., and Wereley, N. M., "Semi-Active Damping of Ground Resonance in Helicopters Using Magnetorheological Dampers," *Journal of the American Helicopter Society*, Vol. 49, No. 4, Oct. 2004, pp. 468–482. doi:10.4050/JAHS.49.468

[14] Titurus, B., and Lieven, N., "Modeling and Analysis of Active Dampers in Periodic Working Environments," *AIAA Journal*, Vol. 47, No. 10, Oct. 2009, pp. 2404–2416. doi:10.2514/1.41774

[15] Knospe, C. R., Hope, R. W., Fedigan, S. J., and Williams, R. D., "Experiments in the Control of Unbalance Response Using Magnetic Bearings," *Mechatronics*, Vol. 5, No. 4, 1995, pp. 385–400. doi:10.1016/0957-4158(95)00015-W

[16] Friedmann, P. P., and Millott, T. A., "Vibration Reduction in Rotorcraft Using Active Control: A Comparison of Various Approaches," *Journal of Guidance, Control, and Dynamics*, Vol. 18, No. 4, July–Aug. 1995, pp. 664–673. doi:10.2514/3.21445

[17] Patt, D., Liu, L., Chandrasekar, J., Bernstein, D. S., and Friedmann, P. P., "Higher-Harmonic-Control Algorithm for Helicopter Vibration Reduction Revisited," *Journal of Guidance, Control, and Dynamics*, Vol. 28, No. 5, Sept.–Oct. 2005, pp. 918–930. doi:10.2514/1.9345

[18] Titurus, B., and Lieven, N., "Integration of Hydraulic Lag Damper Models with Helicopter Rotor Simulations," *Journal of Guidance, Control, and Dynamics*, Vol. 33, No. 1, Jan.–Feb. 2010, pp. 200–211. doi:10.2514/1.41961

[19] Titurus, B., du Bois, J., Lieven, N., and Hansford, R. E., "A Method for the Identification of Hydraulic Damper Characteristics from Steady Velocity Inputs," *Mechanical Systems and Signal Processing*, Vol. 24, No. 8, Nov. 2010, pp. 2868–2887. doi:10.1016/j.ymssp.2010.05.021

[20] *Operating Instructions: MOOG D636 / D638 Series Direct Drive Servo-Proportional Valves with Integrated Digital Electronics and CAN Bus Interface*, CDS6818, Ver. 1.0-US, 04/02, Moog, East Aurora, NY, 2002, .

[21] Ferreira, J. A., Gomes de Almeida, F., and Quintas, M. R., "Semi-Empirical Model for a Hydraulic Servo-Solenoid Valve," *Proceedings of the Institution of Mechanical Engineers, Part I: Journal of Systems and Control Engineering*, Vol. 216, No. 3, 2002, pp. 237–248. doi:10.1243/095965102320005409

[22] MATLAB, Software Package, Ver. 7.4, MathWorks, Natick, MA, 2007.

N. Wereley
Associate Editor